Electronic Supplementary Material (ESI) for Chemical Science.

# Supporting information: Ultrafast Interligand Electron Transfer in cis-[Ru(4,4'-dicarboxylate-2,2'-bipyridine)$_2$(NCS)$_2$]$^{4-}$ and Implications for Electron Injection Limitations in Dye Sensitized Solar Cells

Belinda Pettersson Rimgard,[a] Jens Föhlinger,[a] Jonas Petersson,[a] Marcus Lundberg,[ab] Burkhard Zietz,[a] Ann Marie Woys,[c] Stephen A. Miller,[c] Michael R. Wasielewski,*[c] Leif Hammarström*[a]

[a]Department of Chemistry – Ångström Laboratory, Uppsala University, Box 523, SE75120 Uppsala, Sweden.
[b]Department of Biotechnology, Chemistry and Pharmacy, Università di Siena, Via A. Moro 2, 53100 Siena, Italy.
[c]Department of Chemistry and Argonne-Northwestern Solar Energy Research (ANSER) Center, Northwestern University, Evanston, Illinois 60208-3113, United States.

*E-mail: leif.hammarstrom@kemi.uu.se and m-wasielewski@northwestern.edu

# Contents

# 1 Computational section

## 1.1 Optimized structures

### 1.1.1 $S_0$

The structure of the ground singlet state of N712 was optimized using time-independent B3LYP[1–4]/DGDZVP[5,6]. The calculation incorporated the keyword Nosymm.

**Table S1** $S_0$ structure of N712 optimized using Gaussian 09 (revision D.01).

| | | | |
|---|---|---|---|
| Energy: | -7168.51854253 hartees | | |
| Ru | -1.42017E-05 | -0.000618952 | 0.78600966 |
| N | 0.889680031 | -1.215846609 | -0.681285761 |
| C | 0.282487929 | -2.213986279 | -1.353211477 |
| C | 2.20665749 | -0.964821853 | -0.936104155 |
| C | 0.940389996 | -3.00111409 | -2.292369226 |
| H | -0.763649711 | -2.378264686 | -1.119619218 |
| C | 2.918601579 | -1.727976094 | -1.867355461 |
| C | 2.293382269 | -2.765351936 | -2.5628993 |
| H | 0.410904596 | -3.793229191 | -2.810345241 |
| H | 3.964878358 | -1.534128982 | -2.070885768 |
| N | 1.950206146 | 0.800517287 | 0.672736987 |
| C | 2.800426606 | 0.157601388 | -0.176709977 |
| C | 2.415322187 | 1.84199071 | 1.39049209 |
| C | 4.132953253 | 0.56374944 | -0.306817511 |
| C | 3.72868628 | 2.291394206 | 1.297670211 |
| H | 1.696634092 | 2.314589302 | 2.051435803 |
| C | 4.620074267 | 1.643647689 | 0.433695173 |
| H | 4.812775521 | 0.054501009 | -0.979069033 |
| H | 4.062433798 | 3.135301617 | 1.89146975 |
| N | -0.889629954 | 1.216906325 | -0.679394907 |
| C | -0.282400728 | 2.216163167 | -1.349613048 |
| C | -2.206576041 | 0.966260641 | -0.934745033 |
| C | -0.940237419 | 3.004832634 | -2.287515093 |
| H | 0.763715789 | 2.38006836 | -1.115664379 |
| C | -2.918467831 | 1.730955173 | -1.864777669 |
| C | -2.293210584 | 2.769518728 | -2.558526329 |
| H | -0.41072468 | 3.797815284 | -2.804129087 |
| H | -3.964736416 | 1.537425924 | -2.068678669 |
| N | -1.950237789 | -0.801595911 | 0.671360316 |
| C | -2.800382775 | -0.157396556 | -0.17719298 |
| C | -2.415402645 | -1.844164505 | 1.387487477 |
| C | -4.132871273 | -0.563417046 | -0.308094862 |
| C | -3.728752693 | -2.293444794 | 1.293863069 |
| H | -1.696768049 | -2.317739121 | 2.047790274 |
| C | -4.620047247 | -1.644443806 | 0.430732568 |
| H | -4.812647181 | -0.053206153 | -0.979663497 |
| H | -4.062549755 | -3.138230019 | 1.886384916 |
| N | -0.69066515 | 1.315516722 | 2.264147936 |
| N | 0.690596849 | -1.319021873 | 2.262118536 |
| C | -1.07935569 | 2.044393746 | 3.104296843 |
| C | 1.079112668 | -2.049275338 | 3.101151909 |
| S | 1.613676467 | -3.08001581 | 4.280408171 |
| S | -1.61422417 | 3.073183674 | 4.28511518 |
| C | 6.084260915 | 2.100981541 | 0.300579814 |
| C | 3.068838369 | -3.613336842 | -3.587427216 |
| C | -3.068575734 | 3.619328581 | -3.581613608 |

| | | | |
|---|---|---|---|
| C | -6.084195391 | -2.101640496 | 0.296706351 |
| O | -2.407833669 | 4.527459185 | -4.161877743 |
| O | -4.287904863 | 3.32458418 | -3.738319318 |
| O | -6.804511442 | -1.436641175 | -0.50139871 |
| O | -6.419770178 | -3.097567511 | 0.999173794 |
| O | 6.419697258 | 3.096027987 | 1.004361961 |
| O | 6.804758716 | 1.43694817 | -0.498164219 |
| O | 4.288065305 | -3.317998854 | -3.743838582 |
| O | 2.408270526 | -4.520727187 | -4.169043715 |

### 1.1.2 $T_{1a}$

The lowest excited triplet state was determined using time-independent B3LYP/DGDZVP and Nosymm. This state is referred to as the $T_{1a}$ state due to lowest triplet state being a degenerate state. The states differ depending on which ligand the MLCT state localizes on. The optimized coordinates for the $T_{1a}$ structure is given in Table S2. To be able to compare the determined vibrational transition dipoles moments of $T_{1a}$ structure to the electronic transition dipole moment in $S_0$, the $T_{1a}$ structure had to be transformed onto the $S_0$ structure, subjecting them to the same coordinate system, and the transformed coordinates are given in Table S3. The transformation was done using the VMD RMS based best fit function.[7]

**Table S2** $T_{1a}$ structure of N712 optimized using Gaussian 09 (revision D.01).

| | | | |
|---|---|---|---|
| Energy: | -7168.44720187 hartrees | | |
| Ru | 0.001698938 | -0.854123663 | -0.023778441 |
| N | -0.8379567 | 0.574918207 | 1.218540813 |
| C | -0.203439262 | 1.239155671 | 2.222453918 |
| C | -2.195066261 | 0.832649775 | 0.982724462 |
| C | -0.830958468 | 2.152980525 | 3.036827342 |
| H | 0.846493324 | 0.999144442 | 2.357119833 |
| C | -2.869890302 | 1.766486105 | 1.809243699 |
| C | -2.22253774 | 2.43257658 | 2.832500792 |
| H | -0.282567335 | 2.654196086 | 3.825441417 |
| H | -3.921233767 | 1.976645959 | 1.646542632 |
| N | -1.946705718 | -0.743433542 | -0.798179239 |
| C | -2.790632903 | 0.119355719 | -0.103654115 |
| C | -2.447120797 | -1.469509966 | -1.826664265 |
| C | -4.148379967 | 0.232472833 | -0.504616429 |
| C | -3.760355329 | -1.382863416 | -2.245106391 |
| H | -1.741393249 | -2.131478068 | -2.318540482 |
| C | -4.65126888 | -0.499548176 | -1.563658288 |
| H | -4.818506576 | 0.902130527 | 0.022469803 |
| H | -4.111182345 | -1.97818789 | -3.07986709 |
| N | 0.81982947 | 0.741701573 | -1.133526346 |
| C | 0.143375547 | 1.472035314 | -2.040128062 |
| C | 2.134406849 | 1.013770587 | -0.897297529 |
| C | 0.740622992 | 2.502583579 | -2.75695928 |
| H | -0.898291373 | 1.207463127 | -2.182940388 |
| C | 2.781867809 | 2.039765503 | -1.590108247 |
| C | 2.089767322 | 2.801571442 | -2.535461876 |
| H | 0.168804288 | 3.071058499 | -3.481830193 |
| H | 3.825656131 | 2.268518013 | -1.41256397 |
| N | 1.996530465 | -0.756979125 | 0.723060905 |
| C | 2.793624527 | 0.171138764 | 0.125093598 |
| C | 2.520746664 | -1.562698482 | 1.66434929 |
| C | 4.139947575 | 0.296077587 | 0.480127932 |
| C | 3.853215142 | -1.482016103 | 2.057780638 |

| | | | |
|---|---|---|---|
| H | 1.83998552 | -2.282777993 | 2.105340757 |
| C | 4.69155165 | -0.535702093 | 1.458309088 |
| H | 4.782260757 | 1.030980504 | 0.010197269 |
| H | 4.241230432 | -2.146396267 | 2.821946228 |
| N | 0.705613505 | -2.17407327 | -1.453403101 |
| N | -0.63416591 | -2.345611081 | 1.221709359 |
| C | 1.138299167 | -2.884360612 | -2.293989007 |
| C | -1.017998667 | -3.195607412 | 1.948295137 |
| S | -1.535257462 | -4.376580976 | 2.954106806 |
| S | 1.725271556 | -3.874050958 | -3.457390908 |
| C | -6.116289834 | -0.371351682 | -1.989790565 |
| C | -2.962921642 | 3.435391917 | 3.716986776 |
| C | 2.79509262 | 3.936929512 | -3.304870224 |
| C | 6.174974281 | -0.410404647 | 1.858520362 |
| O | 2.079869663 | 4.565493838 | -4.134189387 |
| O | 4.013220586 | 4.118588496 | -3.025201738 |
| O | 6.831975189 | 0.493611256 | 1.26965824 |
| O | 6.579992663 | -1.225438778 | 2.734295979 |
| O | -6.479655664 | -1.089172917 | -2.971017968 |
| O | -6.839954823 | 0.435765558 | -1.33166351 |
| O | -4.196782509 | 3.613245993 | 3.480339224 |
| O | -2.272974148 | 4.00546663 | 4.617456741 |

**Table S3** T$_{1a}$ structure transformed onto the S$_0$ structure using the VMD RMS based best fit function.

| | | | |
|---|---|---|---|
| Ru | 0.015644 | -0.032432 | 0.839708 |
| N | 0.85853 | -1.16745 | -0.674167 |
| C | 0.236767 | -2.147535 | -1.384456 |
| C | 2.204036 | -0.881553 | -0.941854 |
| C | 0.866808 | -2.890873 | -2.355309 |
| H | -0.804607 | -2.323394 | -1.134029 |
| C | 2.881277 | -1.634612 | -1.934234 |
| C | 2.247137 | -2.634231 | -2.647273 |
| H | 0.328859 | -3.663272 | -2.891848 |
| H | 3.923932 | -1.432466 | -2.153254 |
| N | 1.941431 | 0.797972 | 0.739685 |
| C | 2.78574 | 0.176967 | -0.177091 |
| C | 2.429735 | 1.795477 | 1.515523 |
| C | 4.130521 | 0.619319 | -0.290804 |
| C | 3.730098 | 2.252573 | 1.430046 |
| H | 1.724776 | 2.2295 | 2.217558 |
| C | 4.620644 | 1.64704 | 0.492708 |
| H | 4.800636 | 0.149668 | -1.001934 |
| H | 4.07124 | 3.060388 | 2.066735 |
| N | -0.860862 | 1.145985 | -0.673766 |
| C | -0.221692 | 2.110801 | -1.361876 |
| C | -2.174089 | 0.891468 | -0.935674 |
| C | -0.856607 | 2.870167 | -2.338005 |
| H | 0.820969 | 2.265358 | -1.108038 |
| C | -2.8585 | 1.625281 | -1.907765 |
| C | -2.205275 | 2.631003 | -2.625305 |
| H | -0.314316 | 3.641501 | -2.873301 |
| H | -3.901714 | 1.433932 | -2.12784 |
| N | -1.961257 | -0.824517 | 0.734722 |
| C | -2.790946 | -0.194952 | -0.142542 |
| C | -2.445936 | -1.824317 | 1.493337 |
| C | -4.130066 | -0.577386 | -0.263964 |
| C | -3.769387 | -2.247269 | 1.413601 |

| | | | |
|---|---|---|---|
| H | -1.740495 | -2.288233 | 2.174189 |
| C | -4.640687 | -1.616232 | 0.518998 |
| H | -4.798094 | -0.082722 | -0.958608 |
| H | -4.125125 | -3.058544 | 2.039052 |
| N | -0.698393 | 1.299392 | 2.253208 |
| N | 0.711377 | -1.34506 | 2.244366 |
| C | -1.138294 | 2.085791 | 3.018959 |
| C | 1.129741 | -2.109311 | 3.043515 |
| S | 1.694891 | -3.167884 | 4.154345 |
| S | -1.735129 | 3.174124 | 4.085188 |
| C | 6.07172 | 2.118202 | 0.3635 |
| C | 2.990031 | -3.439425 | -3.713057 |
| C | -2.951563 | 3.446071 | -3.701051 |
| C | -6.115708 | -2.047331 | 0.397026 |
| O | -2.269731 | 4.328887 | -4.292785 |
| O | -4.165548 | 3.145501 | -3.876974 |
| O | -6.804678 | -1.42457 | -0.459211 |
| O | -6.482718 | -2.97916 | 1.166638 |
| O | 6.424075 | 3.065424 | 1.130785 |
| O | 6.795988 | 1.52714 | -0.493438 |
| O | 4.213874 | -3.160559 | -3.898769 |
| O | 2.312082 | -4.323183 | -4.322331 |

### 1.1.3 $T_{1b}$

To generate the guess structure for $T_{1b}$, the initially optimized $T_{1a}$ structure with the charge residing on one of the dcb-ligands (L1) had to be transformed onto the other and vice versa (L1 onto L2, and L2 onto L1). This was performed using the VMD RMS based best fit function. The transformed structure was then optimized using B3LYP/DGDZVP with Nosymm and the coordinates are given in Table S4.

**Table S4** $T_{1b}$ structure optimized using Gaussian 09 (revision D.01).

| | | | |
|---|---|---|---|
| Energy: | -7168.44716404 hartees | | |
| Ru | -0.015085434 | 0.013805202 | 0.823546403 |
| N | -0.86208136 | 1.171730466 | -0.670297931 |
| C | -0.241628431 | 2.159794758 | -1.371196667 |
| C | -2.212734223 | 0.900104652 | -0.927199942 |
| C | -0.878094343 | 2.924798779 | -2.320884483 |
| H | 0.804271005 | 2.32311602 | -1.131273641 |
| C | -2.897119882 | 1.6775679 | -1.895123736 |
| C | -2.264599038 | 2.685205068 | -2.598118977 |
| H | -0.340472327 | 3.701457396 | -2.851668358 |
| H | -3.944431012 | 1.489330034 | -2.103414725 |
| N | -1.940169046 | -0.817525462 | 0.713318661 |
| C | -2.791616706 | -0.171653679 | -0.179031022 |
| C | -2.423043841 | -1.834583386 | 1.466821799 |
| C | -4.139807107 | -0.604470089 | -0.287524064 |
| C | -3.725815202 | -2.285385988 | 1.383314552 |
| H | -1.711736425 | -2.289638512 | 2.148871084 |
| C | -4.625362936 | -1.650138485 | 0.474847062 |
| H | -4.815801235 | -0.112881369 | -0.977928963 |
| H | -4.062343735 | -3.110126885 | 2.000431665 |
| N | 0.866987622 | -1.141673079 | -0.704941948 |
| C | 0.230476979 | -2.094974895 | -1.411371618 |
| C | 2.184626729 | -0.891701677 | -0.948675529 |
| C | 0.87324637 | -2.849092471 | -2.386516896 |
| H | -0.816302126 | -2.245500131 | -1.172325887 |

| | | | |
|---|---|---|---|
| C | 2.87720366 | -1.621558286 | -1.917883337 |
| C | 2.227800503 | -2.617728042 | -2.651841117 |
| H | 0.332625484 | -3.610818403 | -2.937054147 |
| H | 3.924308767 | -1.435497297 | -2.12338266 |
| N | 1.959331016 | 0.812455928 | 0.731710696 |
| C | 2.796313663 | 0.187276421 | -0.14160232 |
| C | 2.436763105 | 1.810964375 | 1.496505865 |
| C | 4.13688386 | 0.569007139 | -0.248897639 |
| C | 3.759895816 | 2.2366132 | 1.42718597 |
| H | 1.72572983 | 2.271391408 | 2.173894794 |
| C | 4.640018244 | 1.60678668 | 0.540370524 |
| H | 4.810729652 | 0.074888885 | -0.938287275 |
| H | 4.108906758 | 3.048019399 | 2.056194052 |
| N | 0.700904399 | -1.34128718 | 2.214091414 |
| N | -0.712257005 | 1.299391979 | 2.252383158 |
| C | 1.140245958 | -2.137517092 | 2.969947867 |
| C | -1.131331351 | 2.042679668 | 3.070674829 |
| S | -1.697798371 | 3.072291373 | 4.207775118 |
| S | 1.736001795 | -3.238897923 | 4.023195804 |
| C | -6.080608766 | -2.110084178 | 0.35250144 |
| C | -3.01788329 | 3.515559653 | -3.636745264 |
| C | 2.986715489 | -3.431543919 | -3.719630107 |
| C | 6.116138539 | 2.038293051 | 0.434023787 |
| O | 2.311435564 | -4.311328975 | -4.323256202 |
| O | 4.203884034 | -3.133554913 | -3.877335956 |
| O | 6.823884356 | 1.390668052 | -0.387729583 |
| O | 6.465301211 | 2.995651906 | 1.180309776 |
| O | -6.425126139 | -3.083543488 | 1.089921963 |
| O | -6.815891595 | -1.484435716 | -0.469781426 |
| O | -4.243604309 | 3.240577007 | -3.816416234 |
| O | -2.346734167 | 4.414179121 | -4.231654628 |

## 1.2 Vibrational modes

### 1.2.1 $S_0$

In addition to the optimization of the structures of the singlet and triplet state, frequency calculations were performed. Nosymm was implemented and the compatible iop(7/33=3) to extract the transition dipole moment derivatives in the output file with input orientation. The computation of the $S_0$ state of N712 contained no imaginary frequencies and in Figure S1 the relevant carboxylate stretching modes are displayed. From the displacement vectors (red arrows) simulated in GaussView 5.0.8, it is evident that the carboxylate stretches are coupled with movement of the bpy-ring.

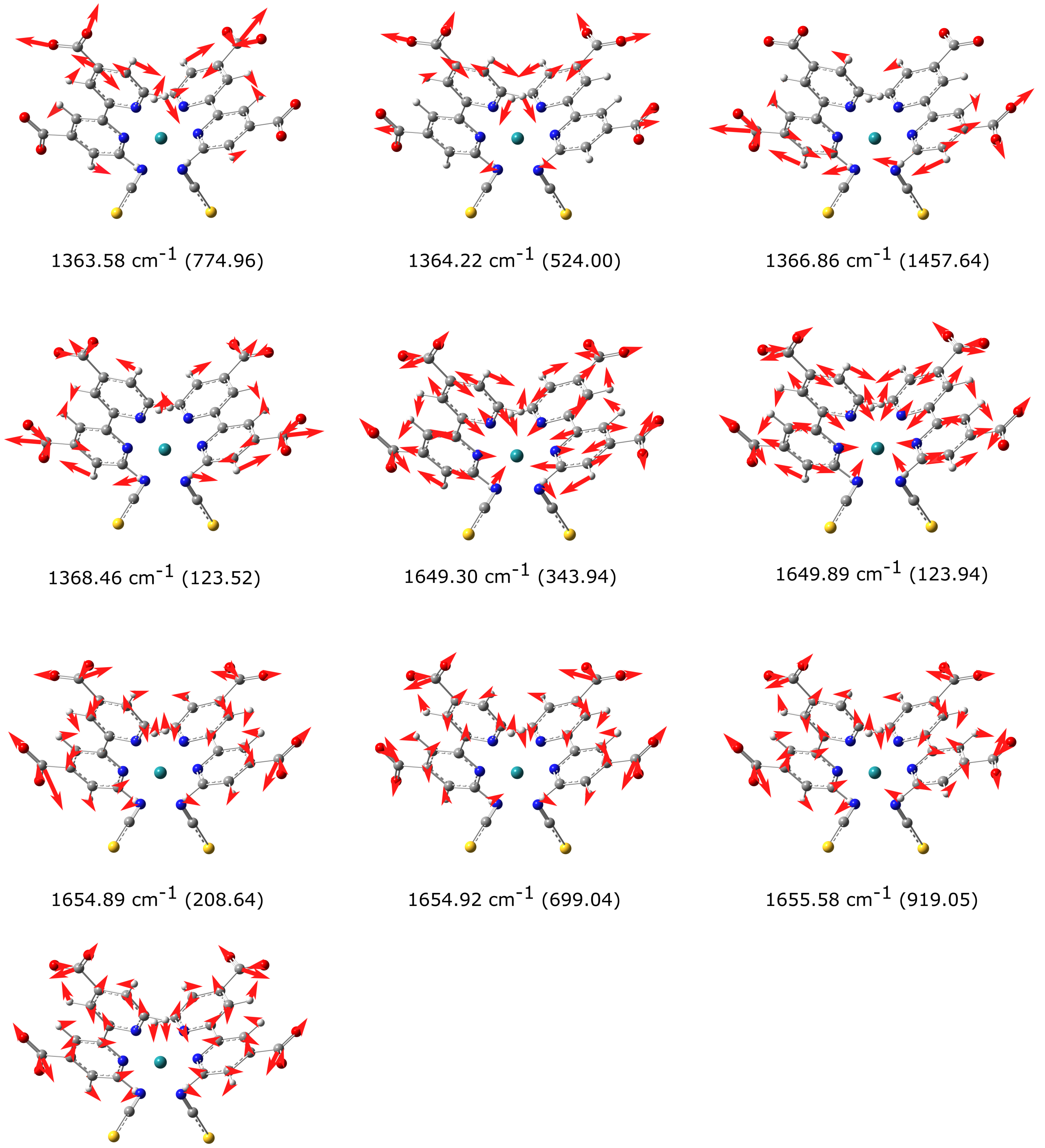

1363.58 cm$^{-1}$ (774.96)

1364.22 cm$^{-1}$ (524.00)

1366.86 cm$^{-1}$ (1457.64)

1368.46 cm$^{-1}$ (123.52)

1649.30 cm$^{-1}$ (343.94)

1649.89 cm$^{-1}$ (123.94)

1654.89 cm$^{-1}$ (208.64)

1654.92 cm$^{-1}$ (699.04)

1655.58 cm$^{-1}$ (919.05)

1655.94 cm$^{-1}$ (276.92)

**Figure S1** Normal vibrational modes involving carboxylate stretches computationally determined for the $S_0$ state of N712. Vibrational displacement vectors of the atoms are given by red arrows and the vibrational frequencies and corresponding intensities (latter in parenthesis) are given as calculated.

### 1.2.2 $T_1$

The optimized structures of the degenerate $T_1$ states ($T_{1a}$ and $T_{1b}$) showed no imaginary frequencies as the IR spectrum was calculated. The calculation procedure followed that of the $S_0$ state calculation, hence using Nosymm and iop(7/33=3). In Figure S2 the displacement vectors of the atoms in red shows that certain vibrational modes are only active on a specific ligand, as well as only involving one carboxylate. Note, that here the vibrations of $T_{1a}$ has been used as reference, considering that $T_{1b}$ shows the same vibrations.

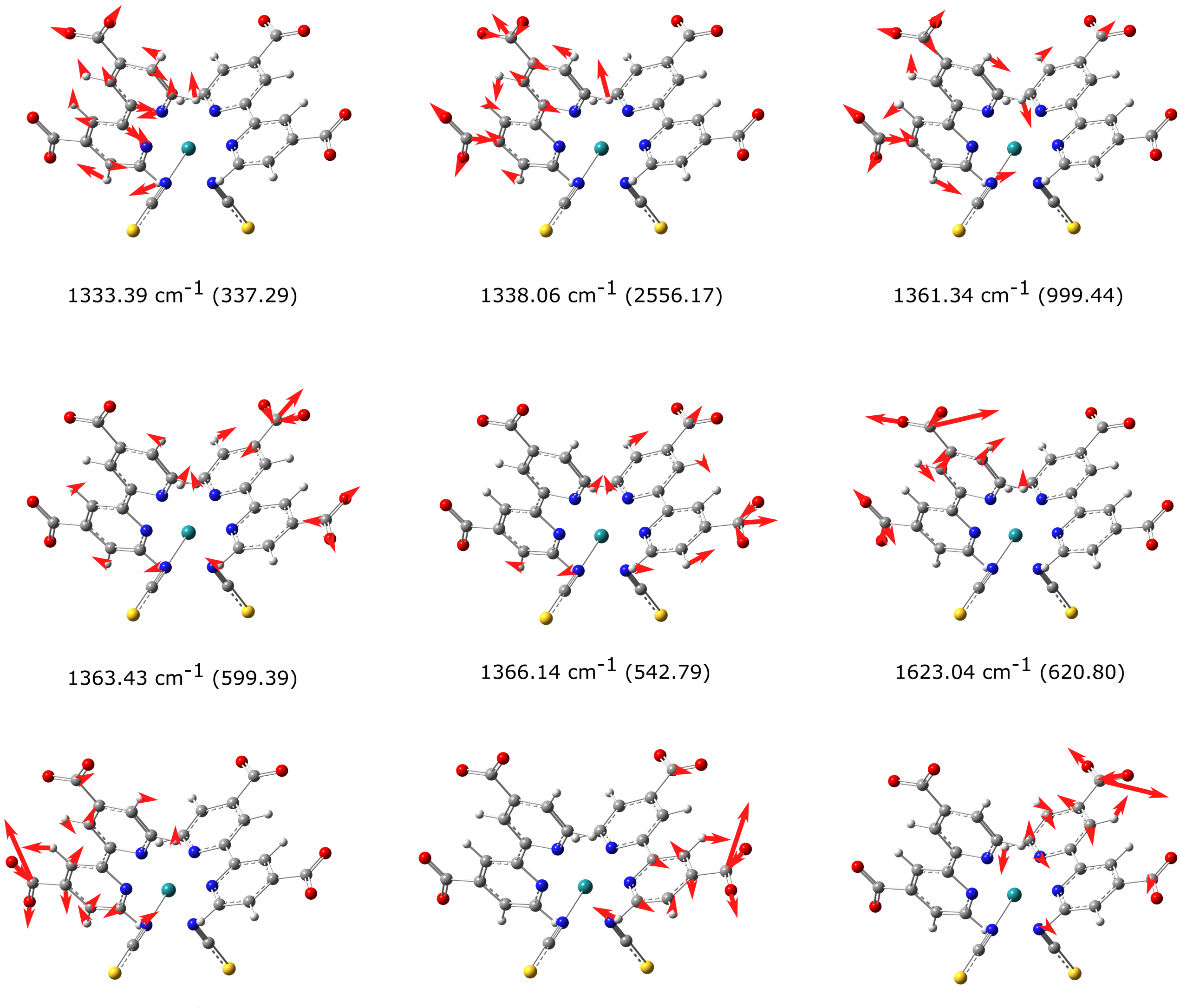

1333.39 $cm^{-1}$ (337.29)

1338.06 $cm^{-1}$ (2556.17)

1361.34 $cm^{-1}$ (999.44)

1363.43 $cm^{-1}$ (599.39)

1366.14 $cm^{-1}$ (542.79)

1623.04 $cm^{-1}$ (620.80)

1630.26 $cm^{-1}$ (610.18)

1659.65 $cm^{-1}$ (542.94)

1661.53 $cm^{-1}$ (625.92)

**Figure S2** Normal vibrational modes involving carboxylate stretches computationally determined for the $T_1$ state of N712.Vibrational displacement vectors of the atoms are given by red arrows and the vibrational frequencies and corresponding intensities (latter in parenthesis) are given as calculated.

## 1.3 Vibrational dipole moment derivatives

The calculated vibrational frequencies and their corresponding intensities and dipole moment derivatives are given in Table S5. The table contains both the direct results of the DFT calculations as well as the transformed vectors, such as in the case of the $T_{1a}$ structure being moved to the same coordinate system as the $S_0$ structure. Additionally, the $T_{1b}$ vectors are given for the ligand transform, hence the switch of the position of the $T_{1a}$ dcb-ligands. This transform consequently changes the location of the MLCT excitation from L1 to L2, consequently forming the degenerate state $T_{1b}$.

**Table S5** Characterization of each carboxylate stretching with correspondingly calculated vibrational dipole moment derivatives (DD). L1 and L2 refer to the two different dcb-ligands, here used to depict where the stretching is taking place. For $T_{1a}$, L1 is the ligand carrying the charge, while for $T_{1b}$ it is L2. All stretches are coupled to movement of the bpy-rings on the concerned ligand.

| Vib | Freq | Freq x0.986 | Feature | Intensity | DD (x) | DD (y) | DD (z) |
|---|---|---|---|---|---|---|---|
| **$S_0$** | | | | | | | |
| **sym** | 1363.58 | 1344.49 | L1-L2 (one carboxylate each) | 774.9593 | -15.5767 | 23.0720 | 0.1061 |
| **sym** | 1364.22 | 1345.12 | L1-L2 (all carboxylates) | 523.9967 | 0.0778 | -0.1016 | 22.8906 |
| **sym** | 1366.86 | 1347.72 | L1-L2 (one carboxylate each) | 1457.6393 | 36.3850 | 11.5660 | -0.0204 |
| **sym** | 1368.46 | 1349.30 | L1-L2 (all carboxylates) | 123.5235 | -0.0626 | -0.0074 | -11.1139 |
| **asym** | 1649.30 | 1626.21 | L1-L2 (all carboxylates) | 343.9433 | -9.6057 | -15.8642 | 0.0002 |
| **asym** | 1649.89 | 1626.79 | L1-L2 (all carboxylates) | 123.9385 | 0.0230 | 0.0092 | 11.1327 |
| **asym** | 1654.89 | 1631.72 | L1-L2 (all carboxylates) | 208.6374 | -2.3044 | 0.3217 | 14.2557 |
| **asym** | 1654.92 | 1631.75 | L1-L2 (all carboxylates) | 699.0444 | 26.2087 | -3.2535 | 1.2496 |
| **asym** | 1655.58 | 1632.40 | L1-L2 (all carboxylates) | 919.0505 | 11.8363 | 27.9095 | 0.1044 |
| **asym** | 1655.94 | 1632.76 | L1-L2 (all carboxylates) | 276.9188 | -0.0727 | -0.1937 | 16.6396 |
| **$T_{1a}$** | | | | | | | |
| **sym** | 1333.39 | 1314.72 | L1 (one carboxylate) | 337.2857 | 0.0694 | -12.7019 | -13.2643 |
| **sym** | 1338.06 | 1319.33 | L1 (two carboxylates) | 2556.1713 | 20.3634 | 25.0637 | 38.9013 |
| **sym** | 1361.34 | 1342.28 | L1-L2 (all carboxylates, weak L2) | 999.4438 | 31.2754 | -3.9828 | -2.3304 |
| **sym** | 1363.43 | 1344.34 | L2-L1 (all carboxylates, weak L1) | 599.3876 | -7.2383 | 18.1714 | -14.7239 |
| **sym** | 1366.14 | 1347.01 | L2-L1 (all carboxylates, weak L1) | 542.7928 | 20.4930 | 10.9405 | 1.7707 |
| **asym** | 1623.04 | 1600.32 | L1 (two carboxylates, one weak) | 620.8038 | 23.8027 | -0.9529 | 7.3026 |
| **asym** | 1630.26 | 1607.44 | L1 (two carboxylates, one weak) | 610.1769 | -0.4247 | 16.0046 | 18.8109 |
| **asym** | 1659.65 | 1636.41 | L2 (two carboxylates, one weak) | 542.9422 | 7.8263 | 17.5259 | -13.2111 |
| **asym** | 1661.53 | 1638.27 | L2 (two carboxylates, one weak) | 625.9201 | 20.7561 | -5.5567 | 12.8152 |
| **$T_{1a}$ (transformed)** | | | | | | | |
| **sym** | 1333.39 | 1314.72 | L1 (one carboxylate) | 337.2857 | -0.1563 | 12.4935 | 13.4395 |
| **sym** | 1338.06 | 1319.33 | L1 (two carboxylates) | 2556.1713 | -19.8568 | -37.9128 | -26.9390 |
| **sym** | 1361.34 | 1342.28 | L1-L2 (all carboxylates, weak L2) | 999.4438 | -31.2399 | 1.2672 | 4.6549 |
| **sym** | 1363.43 | 1344.34 | L2-L1 (all carboxylates, weak L1) | 599.3876 | 6.5141 | 15.9296 | -17.4213 |
| **sym** | 1366.14 | 1347.01 | L2-L1 (all carboxylates, weak L1) | 542.7928 | -20.6481 | -1.6785 | -10.6722 |
| **asym** | 1623.04 | 1600.32 | L1 (two carboxylates, one weak) | 620.8038 | -23.5870 | -7.9747 | 0.9350 |
| **asym** | 1630.26 | 1607.44 | L1 (two carboxylates, one weak) | 610.1769 | 0.5902 | -17.8417 | -17.0947 |
| **asym** | 1659.65 | 1636.41 | L2 (two carboxylates, one weak) | 542.9422 | -8.4923 | 13.9869 | -16.5967 |
| **asym** | 1661.53 | 1638.27 | L2 (two carboxylates, one weak) | 625.9201 | -20.3142 | -13.6627 | 5.1541 |
| **$T_{1b}$** | | | | | | | |
| **sym** | 1333.47 | 1314.80 | L2 (one carboxylate) | 488.3472 | -0.9230 | -15.7706 | 15.4526 |
| **sym** | 1338.00 | 1319.27 | L2 (two carboxylates) | 2422.9994 | 19.4736 | 37.3819 | -25.4238 |
| **sym** | 1361.38 | 1342.32 | L2-L1 (all carboxylates, weak L1) | 954.4940 | 30.6132 | -4.1030 | 0.7009 |
| **Sym** | 1362.73 | 1343.65 | L1-L2 (all carboxylates, weak L2) | 689.1672 | 10.9196 | 15.1702 | 18.4336 |
| **sym** | 1365.87 | 1346.75 | L1-L2 (all carboxylates, weak L2) | 504.8449 | 20.2196 | 2.8137 | -9.3860 |
| **asym** | 1622.61 | 1599.89 | L2 (two carboxylates, one weak) | 622.4921 | 23.6136 | 8.0268 | 0.6771 |
| **asym** | 1630.15 | 1607.33 | L2 (two carboxylates, one weak) | 610.1698 | -1.0323 | 18.4531 | -16.3886 |
| **asym** | 1659.91 | 1636.67 | L1 (two carboxylates, one weak) | 539.2570 | -10.2102 | 13.8438 | 15.5999 |
| **asym** | 1661.23 | 1637.97 | L1 (two carboxylates, one weak) | 637.0978 | 19.5824 | 14.5694 | 6.4311 |
| **$T_{1b}$ ($T_{1a}$ ligand transform)** | | | | | | | |
| **sym** | 1338.06 | 1319.33 | L2 (two carboxylates) | 2556.1713 | 19.9488 | 38.2220 | -26.4115 |
| **asym** | 1623.04 | 1600.32 | L2 (two carboxylates, one weak) | 620.8038 | 23.6127 | 7.8680 | 7.8680 |

## 1.4 Calculation of the initial anisotropy

The calculations of the initial anisotropy of the localized MLCT state compared to that of a random mixture of localized MLCT states, makes the assumption that the electronic transition dipole moment can be estimated as a vector bisecting one of the bipyridyl-ligands. This assumption is based on previous work showing the $^3$MLCT state localizing on one ligand.[8–10] It should however be noted that the NCS ligands, having significant electron density in the HOMO, may have a certain influence on the direction of the excitation dipole moment that has not been considered here.

The electronic transition dipole moment is estimated from the $S_0$ structure; the placement vectors of the two bridging carbons (C4 and C12) and the Ru atom (Table S6). The calculation is a mere translation of the system moving ruthenium into the origin and a subsequent resulting vector construction from the carbon vectors.

**Table S6** Atom vectors for ruthenium, carbon 4 and carbon 12, attained from the $S_0$ structure of N712.

| Atom | X | Y | Z |
|---|---|---|---|
| C4 | 2.20665749 | -0.964821853 | -0.936104155 |
| C12 | 2.800426606 | 0.157601388 | -0.176709977 |
| Ru1 | -1.42017E-05 | -0.000618952 | 0.78600966 |

The translation of ruthenium into the origin and the corresponding vectors to the carbons from ruthenium is determined by subtraction of the ruthenium vector.

C4-Ru: 2.206671692(X) -0.9642029(Y) -1.722113815(Z)
C12-Ru: 2.800440808(X) 0.15822034(Y) -0.962719637(Z)
Ru-Ru: 0(X) 0(Y) 0(Z)

Determination of the resulting vector is the sum of the translated carbon vectors (C4 and C12).

Resulting vector: 5.0071125(X) -0.80598256(Y) -2.684833452(Z)
Normalized: 0.872564069(X) -0.140454488(Y) -0.467872292(Z)

With the normalized excitation dipole moment determined, the vibrational dipole moment vectors were determined from the Gaussian outputs. The symmetrical stretch considered in the paper at 1327 $cm^{-1}$ was found to correspond to the calculated 1338 $cm^{-1}$ stretch (unscaled).

**Table S7** Vibrational transition dipole moment vectors, DD (nDD for normalized), for the considered symmetrical stretch, 1338 $cm^{-1}$ (unscaled), centred at either ligand L1 ($T_{1a}$) or on the other dcb-ligand, L2 ($T_{1b}$). $T_{1b}$ was calculated either from Gaussian or as a transform of $T_{1a}$.

| MLCT state | Intensity | DD(x) | DD(y) | DD(z) | nDD(x) | nDD(y) | nDD(z) |
|---|---|---|---|---|---|---|---|
| $T_{1a}$ | 2556.1713 | -19.8568 | -37.9128 | -26.9390 | -0.3927 | -0.7497 | -0.5327 |
| $T_{1b}$ (DFT) | 2422.9994 | 19.4736 | 37.3819 | -25.4238 | 0.3956 | 0.7594 | -0.5165 |
| $T_{1b}$ (Transform) | 2556.1713 | 19.9490 | 38.2220 | -26.4115 | 0.3945 | 0.7559 | -0.5224 |

From the normalized transition dipole moment vectors ($\mu_{el,norm}$ and $\mu_{vib,norm}$) the scalar/dot product is determined and the anisotropy calculated according to Equation 1. The determined anisotropies given in Table S8 are the predicted initial anisotropies of the localized and the randomized MLCT state. The initial anisotropy of the localized state is given by the anisotropy calculated for the $T_{1a}$ state, since this is the state formed after the photoselection. The anisotropies calculated for the $T_{1b}$ state (DFT/Transform) are used to calculated the predicted anisotropy of the randomized state, which is given by the weighted sum of the initial anisotropies. Hence, the anisotropy of the $T_{1a}$ is weighted by its fractional intensity ($f_i$) and summed with the weighted initial anisotropy calculated for the $T_{1b}$ state (either DFT or Transform). The calculation is performed according to Equation 2.

$$r = \frac{1}{5}(3cos^2\theta - 1) = \frac{1}{5}(3(\mu_{el,norm} \bullet \mu_{vib,norm})^2 - 1) \tag{1}$$

$$r_{obs} = \sum_{i=1}^{n} f_i r_i = \sum_{i=1}^{n} (\frac{I_i}{\sum_{j=1}^{m} I_j}) r_i \qquad n = m \tag{2}$$

**Table S8** Calculated scalar products and the resulting initial anisotropies for the localized and randomized states at 1338 $cm^{-1}$ (unscaled). The initial anisotropy of the $T_{1a}$ is associated to the photoselection, meaning it is considered the maximum anisotropy of the localized state. The initial anisotropy of the $T_{1b}$ state (DFT/Transform) is used in the weighted sum of anisotropies, including the contribution from the $T_{1a}$ state, to determined the maximum initial anisotropy for a randomized state.

| **MLCT state** | $(\mu_{el,norm} \cdot \mu_{vib,norm})$ | $(\mu_{el,norm} \cdot \mu_{vib,norm})^2$ | $\mathbf{r}_{loc}$ | $\mathbf{r}_{rand}$ |
|---|---|---|---|---|
| $T_{1a}$ | 0.011918 | 0.000142 | **-0.1999** | |
| $T_{1b}$ (DFT) | 0.480185 | 0.230578 | -0.0616 | **-0.1326** |
| $T_{1b}$ (Transform) | 0.482492 | 0.232798 | -0.0603 | **-0.1301** |

If performing a similar calculation for a delocalized electronic transition dipole moment, using the unit vector (3.72544E-05, 0.000806558, -0.999999674), directed in between the two dcb ligands, the resulting initial anisotropy is roughly -0.03 for both the localized and the randomized state. This arises from the fact that for a delocalized excitation both vibrational transition dipole moments (T1a and T1b) are 60 degrees from the excitation vector, resulting in identical contributions to the anisotropy. The anisotropy of the randomized state is determined by a weighted average, and since the intensities of the vibrations are almost identical from the DFT calculations the anisotropy becomes equal to the one determined for the localized state.

## 1.5 Anisotropy Effects of Overlapping Ground State Bleach

The influence of the GSB on the predicted anisotropy at 1338 $cm^{-1}$ (experimental 1327 $cm^{-1}$) is estimated by considering the anisotropy of the S0 vibrations: 1363.58 (positive anisotropy), 1364.22 (negative anisotropy) and 1366.86 $cm^{-1}$ (positive anisotropy). They are roughly 25 $cm^{-1}$ away from 1338 $cm^{-1}$, which would indicate only minor effects on the anisotropy. To determine their relative intensities at the 1338 $cm^{-1}$ a Lorentzian line shape was assumed for each peak, as well as a FWHM of 25 $cm^{-1}$ (estimated from the FTIR spectrum). This width is most likely larger than the true FWHM of the peaks and the Lorentzian line shape has longer wings than the Gaussian line shape,[11] meaning that the calculated effect of the GSB will be overestimated (upper limit). The corresponding intensities at 1338 $cm^{-1}$ were 149, 97 and 230. The final, weighted, anisotropy values at 1338 $cm^{-1}$, corresponding to 1327 $cm^{-1}$ in the experimental spectrum, becomes -0.15 for localized and -0.11 for randomized. Thus, GSB contribution is too small to make the experimental anisotropy consistent with a localized state. Instead, GSB may contribute to make the experimental anisotropy less negative than the predicted value of -0.13 for the randomized state.

# 2 Reference measurement

## 2.1 9-cyanoanthracene

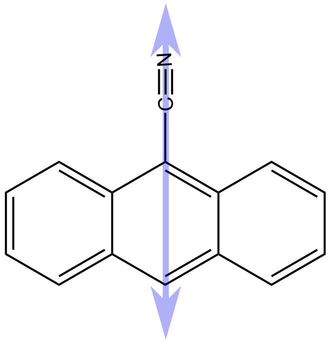

**Figure S3** Structure of 9-cyanoanthracene with the direction of the excitation dipole moment given in blue.

To ensure the accuracy of the relative polarizations in the anisotropy measurements, 9-cyanoanthracene was used as a reference. This compound has recently been studied by Koch *et al.* were the initial anisotropy was predicted to be 0.40, due to the parallel excitation and vibrational transition dipole moments bisecting the cyano-group (see Figure S3).[12] Koch determined an initial anisotropy of 0.34 with a 9 ps time constant. The fitting procedure was performed from the first 500 fs, due to a prominent artefact at earlier times. The corresponding measurements in this study resulting in the transient anisotropy spectrum shown in Figure S4 and the fitted trace in Figure S5. The 9-cyanoanthracene was used as purchased (Sigma Aldrich) in deuterated acetonitrile (Sigma Aldrich) with a final absorption of 0.3 at 410 nm ($E_{exc}$: 0.4 $\mu$J). The isotropic spectrum in Figure S4 shows a peak around 2130 $\text{cm}^{-1}$ corresponding to the CN stretch. The anisotropy in Figure S5 at two frequencies (2128 and 2130 $\text{cm}^{-1}$) was fitted using global analysis and a single exponential function with a resulting time constant of 9.5 ps (±1.6 ps) and an initial anisotropy at time zero slightly above 0.40. The anisotropy slightly above 0.40 is explained by the extrapolation as well as a possible small error introduced by the weighting of the parallel and perpendicular traces, besides the overall noise in the measurement. The trace reveals the presence of a similar artefact as that found by Koch at times before 500 fs and due to issues in fitting this artefact, no chirp correction was performed. Based on these results however, the relative polarization of the pump and probe was considered sufficient.

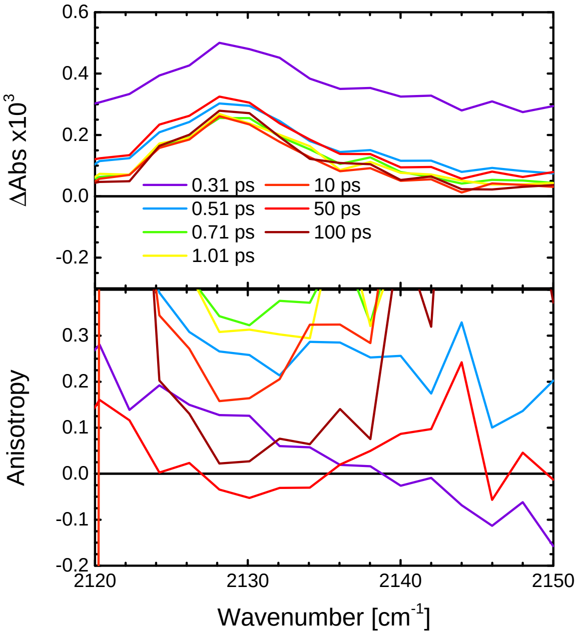

**Figure S4** Transient femtosecond mid-IR spectra of 9-cyanoanthracene in MeCN-$d_3$ excited using 410 nm laser light. Top: transient spectrum in the region of the CN-stretch (2130 cm$^{-1}$) of the total absorption divided by three. Bottom: transient anisotropy spectrum constructed from the parallel and perpendicular traces, in the corresponding region.

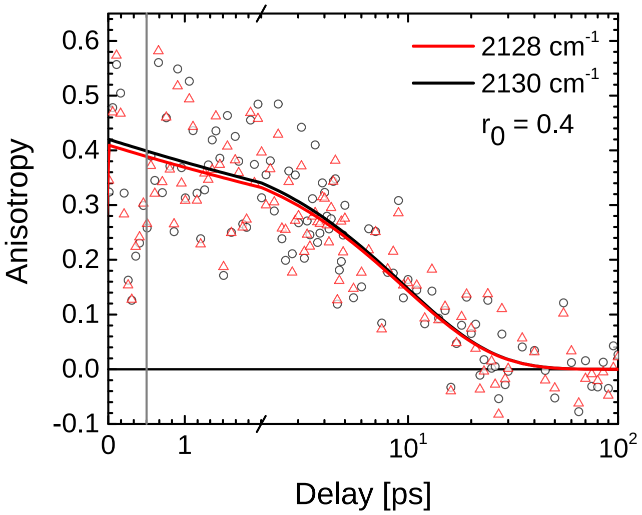

**Figure S5** Transient anisotropy anisotropy traces of 9-cyanoanthracene in MeCN-$d_3$ excited at 410 nm, probed in the region of the CN-stretch (2128 and 2130 cm$^{-1}$). The traces were fitted through global analysis and the time constant found was 9.5 ps (±1.6 ps) with initial anisotropies of 0.41 and 0.42, respectively. Fitting was subjected to times after 500 fs (gray line) due to an intrinsic artefact.

# 3 Characterization of N712

## 3.1 UV-Vis and FTIR

The UV-Vis spectrum (Figure S6) was collected as well as the FTIR (Figure S7), enabling the determination of a suitable excitation wavelength and probe region. The experiments were performed exciting at a tailband (650 nm) to lower the excess excitation energy and therefore lowering the amount of possible overlapping bands. The IR probe region was subjected to the symmetrical stretch of the carboxylate groups (1347 $cm^{-1}$), due to the low presence of overlapping bands indicated by the calculations.

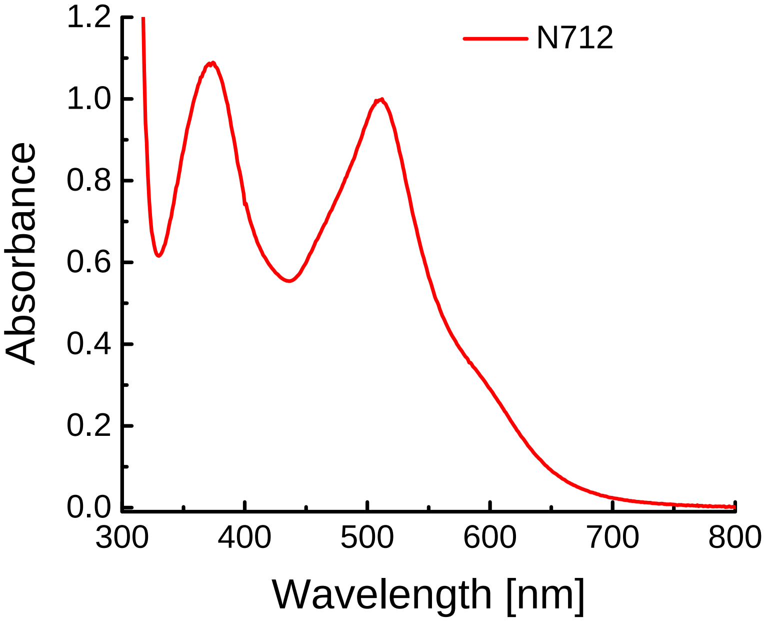

**Figure S6** Steady-state UV-Vis absorption spectrum of N712 in deuterated MeCN.

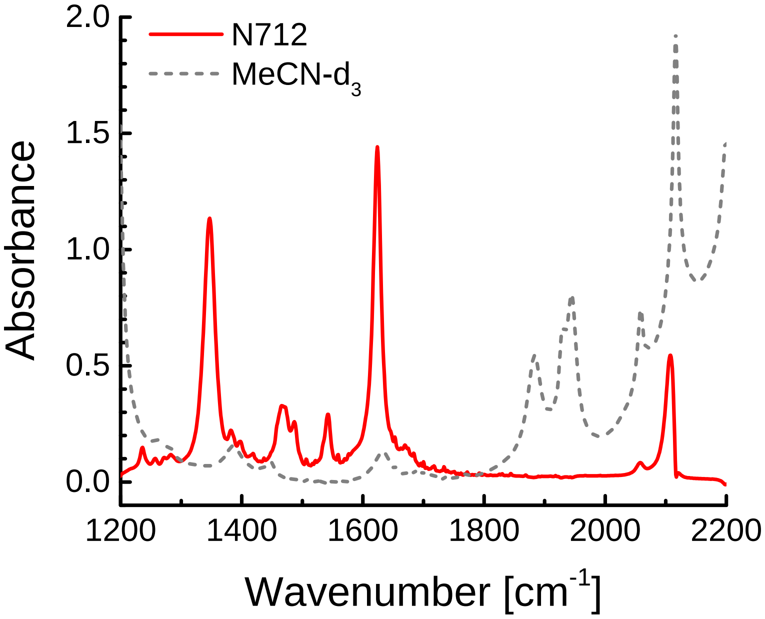

**Figure S7** FTIR spectrum of N712 in deuterated MeCN (red). The solvent FTIR spectrum is given by the gray dashed line.

# 4 Polarized measurements of N712

## 4.1 Parallel and perpendicular infrared absorption spectra

The transient femtosecond mid-IR spectrum of the calculated isotropical signal corresponding to a magic angle measurement, is given in the paper. The underlying parallel and perpendicular spectra used to construct the isotropic signal as well as to determine the anisotropy, are given in Figure S8. The perpendicular signal (bottom) shows a larger magnitude than that compared to parallel, explaining the negative signal seen in the anisotropy. The parallel and perpendicular signals were weighted to ensure that the rotational diffusion causes a zero anisotropy, therefore excluding the influence of possible laser fluctuations.

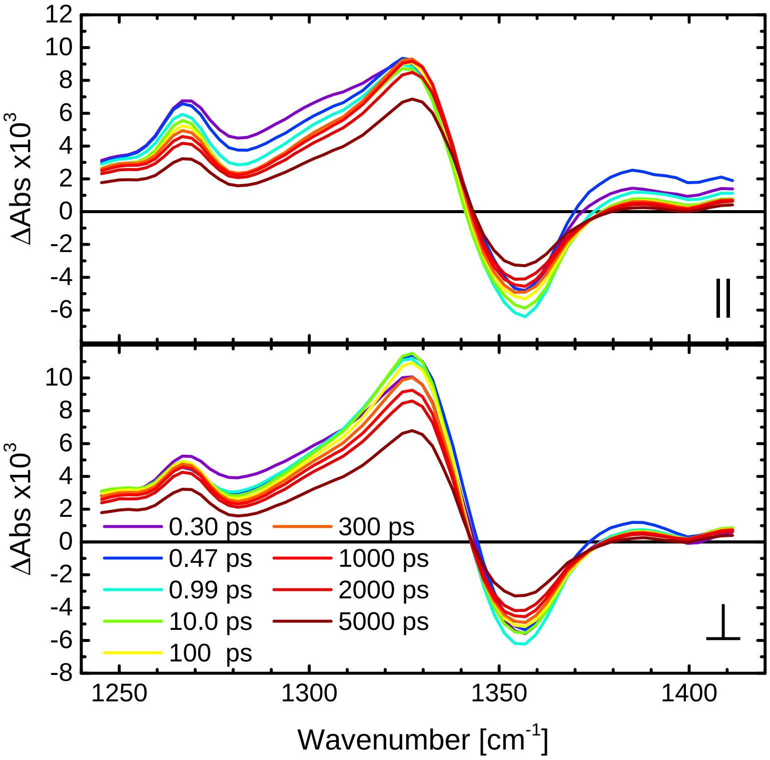

**Figure S8** Parallel (top) and perpendicular (bottom) transient mid-IR absorption spectra of N712 in deuterated MeCN in the symmetric stretch region of the carboxylates (1327 cm$^{-1}$). The excitation wavelength used was 650 nm (0.7 $\mu$J).

## 4.2 Calculated Magic Angle infrared absorption traces

The magic angle traces between 1250 and 1365 $\mathrm{cm}^{-1}$ were subjected to global analysis to verify that a short time component could be found similar to that seen in the anisotropy of N712 around 1327 $\mathrm{cm}^{-1}$ (see paper, Fig. 7). In Figure S9 three selected traces are shown: 1267 (ESA), 1327 (ESA) and 1367 (GS and ESA overlap) $\mathrm{cm}^{-1}$ with the corresponding fits given as solid lines. The global analysis performed from 0.5 ps (gray line in figure) to 50 ps resulted in two time constants: 0.81 and 8.09 ps. Hence, at early times there are two rapid time components that are associated to the suggested vibrational energy relaxation seen in the anisotropy at 1327 $\mathrm{cm}^{-1}$ in the paper.

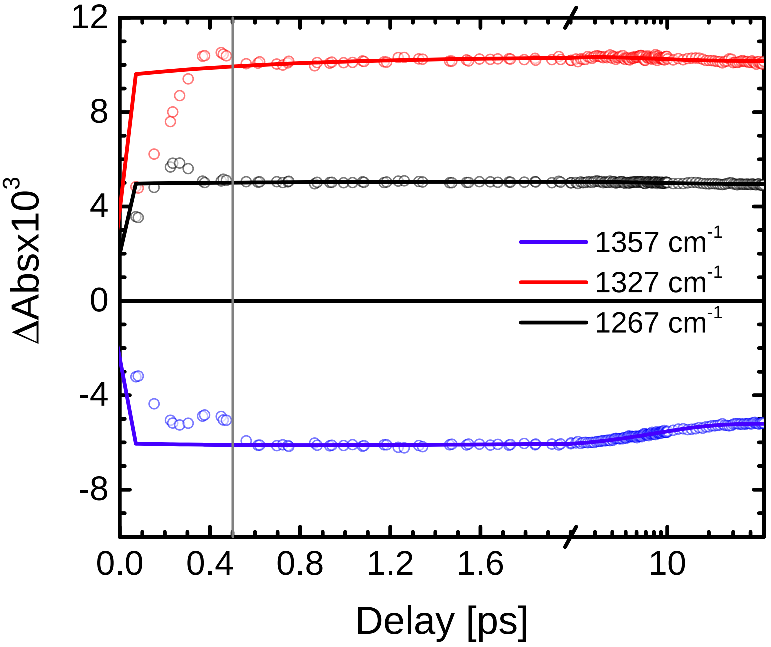

**Figure S9** Constructed magic angle traces of N712 in deuterated MeCN. The traces were subjected to a global fit spanning from 1250 to 1365 $\mathrm{cm}^{-1}$, starting at 0.5 ps (marked in gray) and ending at 50 ps. The fit (solid line) required two time constants: $\tau_1$=0.81 ps and $\tau_2$=8.09 ps. The excitation wavelength used was 650 nm (0.7 $\mu$J).

## 4.3 Rotational correlation time

To determine the time constant for rotational correlation of N712 time-resolved photoluminescence (TRPL) was used measured with a streak camera setup (Hamamatsu C4334 Streakscope) at Northwestern University. The instrument response function (IRF) was approximately 2% of the sweep window. A commercial direct diode-pumped 100 kHz amplifier (Spirit 1040-4, Spectra Physics) produced a fundamental beam of 1040 nm (350 fs, 4.5 W). This light was used to pump a non-collinear optical parametric amplifier (Spirit-NOPA, Spectra-Physics) which delivers high repetition rate pulses. The sample was excited with 600 nm, 100 fs, 20 nJ pulses. The excitation wavelength differs from the one used in the paper (650 nm) due to the absorption being too weak. A polarizer was used after the sample to get the parallel and perpendicular spectra. The spectra between 740-780 nm were averaged to obtain the analyzed parallel and perpendicular traces (see Figure S10) and the anisotropy trace was then calculated and fitted to a monoexponential decay (see Figure S11). The anisotropy was corrected for any preferential diffraction in the spectrograph. Both orientations are included: the top curve assumes that the absorption and emission transition dipole moments are parallel, while the bottom curve assumes they are perpendicular. Note that here the anisotropy amplitude has not been rescaled to zero as previous results and therefore gives the impression that the anisotropy does not go to zero. However it is clear the anisotropy levels off, which if scaled would bring it to zero.

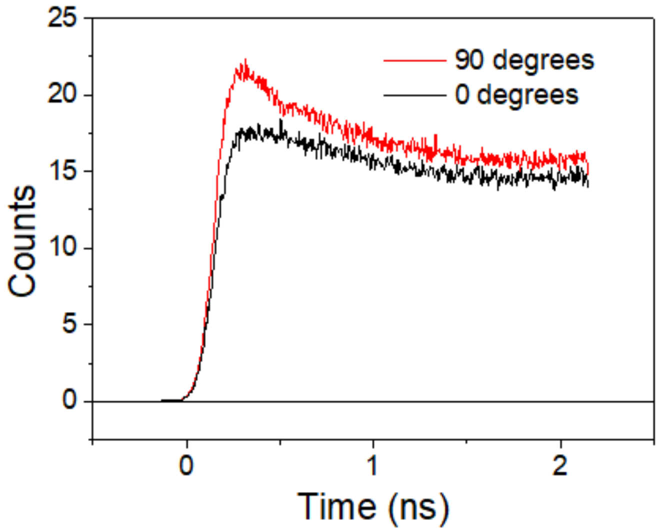

**Figure S10** Parallel and perpendicular transient emission spectra of N712 in deuterated MeCN excited at 600 nm (20 nJ).

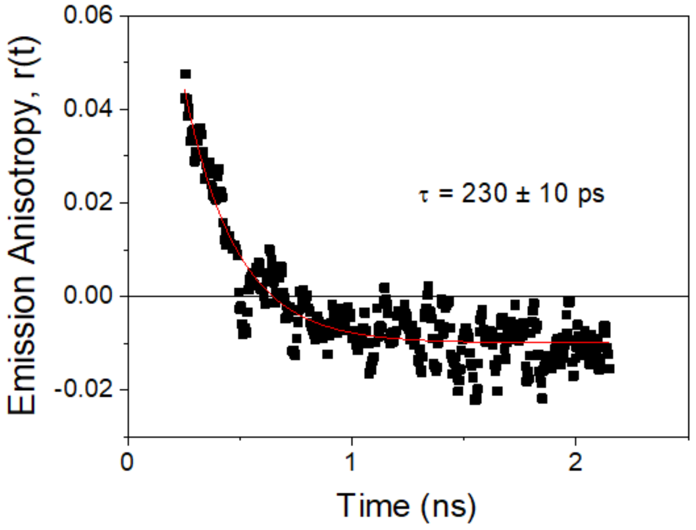

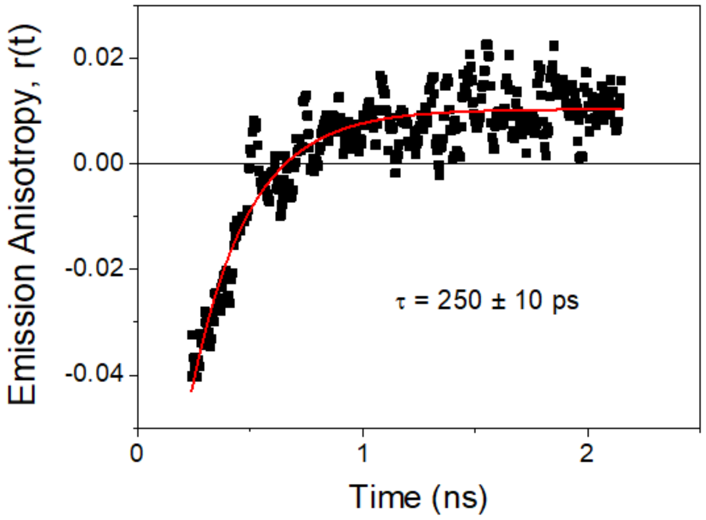

**Figure S11** Anisotropy traces of the transient emission of N712 in deuterated MeCN. On the top the absorption and emission dipole momements are assumed to be parallel. On the bottom they are assumed to be perpendicular.

# 5 Error Analysis

The discrepancy of the calculated anisotropy and the experimentally determine arises from the inherent errors in the procedure. Besides the inherent errors in the DFT calculations, as well as the assumptions attributed to the anisotropy predictions, there are experimental errors that should be considered. The probe laser fluctuation error were estimated using the noise level at times before time zero in the respective parallel and perpendicular traces at various wavenumbers. The standard deviation of the signals at -30 to -1 ps was calculated, seeing an increase in the value when approaching -1 ps. The largest standard deviation found was 0.0001 for both parallel and perpendicular, which was used to determine the upper error margin. The error was determine using a general propagation of error function for multiple variables (Equation 3 for two variables). Here X and Y are representatives of the parallel and perpendicular signals and their respective errors, $\delta X$ and $\delta Y$, are 0.0001. The results show an increasing error towards 1345 cm$^{-1}$ due to the approaching isosbestic point (Table 3). Likewise, going towards 1316 cm$^{-1}$, the error increases. In between these points, the error reaches a minimum at 1327 cm$^{-1}$. To avoid the influence of the isosbestic point to the anisotropy, analysis was subjected to wavenumbers which error showed no major changes considering the neighbouring wavenumbers.

$$\delta F(X,Y) = \sqrt{\left(\frac{\partial F(X,Y)}{\partial X} \cdot \delta X\right)^2 + \left(\frac{\partial F(X,Y)}{\partial Y} \cdot \delta Y\right)^2} \tag{3}$$

The anisotropy of 1327 cm$^{-1}$, the peak of the symmetric carboxylate stretch, show experimentally a lower anisotropy (-0.095) compared to the calculated for both a randomized (-0.13) and localized (-0.20) MLCT state. That the experimental values would arise from a localized state becomes questionable; considering the reference measurement of 9-cyanoanthracene, where the experimental $r_0$ would require a 20° angle error between pump and probe (see Equation 1), and the small laser fluctuation error (see Table 3). The error analysis show that the experimentally determined anisotropies are fairly certain and removes possible doubt of the experimental procedure.

**Table S9** Error analysis of the probe fluctuation at various wavenumbers around the symmetric stretch of the carboxylates (1327$cm^{-1}$) at specific times at the plateau of the anisotropy. The error analysis is based on the standard deviation of the parallel and perpendicular signals between -30 to -1 ps for all measured wavelengths.

| Wavenr.[cm$^{-1}$] / Time [ps] | 1343.18 | 1340.48 | 1337.79 | 1335.11 | 1332.45 | 1329.79 | 1327.14 | 1324.50 | 1321.88 | 1319.26 | 1316.66 |
|---|---|---|---|---|---|---|---|---|---|---|---|
| 6.74 | 1.06982 | 0.02039 | 0.00920 | 0.00629 | 0.00485 | 0.00426 | 0.00405 | 0.00408 | 0.00436 | 0.00470 | 0.00509 |
| 6.82 | 0.95501 | 0.02042 | 0.00919 | 0.00631 | 0.00487 | 0.00428 | 0.00406 | 0.00410 | 0.00437 | 0.00471 | 0.00511 |
| 6.93 | 0.95756 | 0.02047 | 0.00919 | 0.00629 | 0.00486 | 0.00427 | 0.00406 | 0.00410 | 0.00438 | 0.00472 | 0.00511 |
| 7.03 | 1.59938 | 0.01990 | 0.00900 | 0.00617 | 0.00476 | 0.00419 | 0.00399 | 0.00403 | 0.00431 | 0.00464 | 0.00505 |
| 7.14 | 1.49871 | 0.02000 | 0.00905 | 0.00622 | 0.00480 | 0.00421 | 0.00402 | 0.00406 | 0.00433 | 0.00467 | 0.00507 |
| 7.24 | 1.84939 | 0.01982 | 0.00902 | 0.00618 | 0.00479 | 0.00421 | 0.00401 | 0.00405 | 0.00433 | 0.00467 | 0.00507 |
| 7.33 | 2.84502 | 0.01965 | 0.00893 | 0.00614 | 0.00476 | 0.00418 | 0.00399 | 0.00403 | 0.00431 | 0.00464 | 0.00504 |
| 7.42 | 2.16949 | 0.01969 | 0.00898 | 0.00618 | 0.00478 | 0.00421 | 0.00401 | 0.00406 | 0.00434 | 0.00467 | 0.00508 |
| 7.54 | 1.47872 | 0.01984 | 0.00906 | 0.00622 | 0.00481 | 0.00423 | 0.00403 | 0.00407 | 0.00435 | 0.00469 | 0.00509 |
| 7.63 | 1.37677 | 0.02000 | 0.00902 | 0.00621 | 0.00480 | 0.00423 | 0.00402 | 0.00407 | 0.00434 | 0.00468 | 0.00508 |
| 7.73 | 1.34342 | 0.02008 | 0.00911 | 0.00626 | 0.00484 | 0.00425 | 0.00404 | 0.00409 | 0.00436 | 0.00470 | 0.00511 |
| Average | 1.55848 | 0.02002 | 0.00907 | 0.00623 | 0.00481 | 0.00423 | 0.00403 | 0.00407 | 0.00434 | 0.00468 | 0.00508 |

# References

[1] A. D. Becke, *J. Chem. Phys.*, 1993, **98**, 5648–5652.

[2] C. Lee, W. Yang and R. Parr, *Phys. Rev. B*, 1988, **37**, 785–789.

[3] S. H. Vosko, L. Wilk and M. Nusair, *Can. J. Phys.*, 1980, **58**, 1200–1211.

[4] P. Stephens, F. Devlin, C. Chabalowski and M. J. Frisch, *J. Phys. Chem.*, 1994, **98**, 11623–11627.

[5] N. Godbout, D. R. Salahub, J. Andzelm and E. Wimmer, *Can. J. Chem.*, 1992, **70**, 560–571.

[6] C. Sosa, J. Andzelm, B. C. Elkin, E. Wimmer, K. D. Dobbs and D. A. Dixon, *J. Phys. Chem.*, 1992, **96**, 6630–6636.

[7] W. Humphrey, A. Dalke and K. Schulten, *J. Mol. Graphics*, 1996, **14**, 33–38.

[8] N. H. Damrauer, G. Cerullo, A. Yeh, T. R. Boussie, C. V. Shank and J. K. McCusker, *Science*, 1997, **275**, 54–57.

[9] J. K. McCusker, *Acc. Chem. Res.*, 2003, **36**, 876–887.

[10] D. W. Thompson, A. Ito and T. J. Meyer, *Pure Appl. Chem.*, 2013, **85**, 1257—-1305.

[11] J. M. Hollas, *Modern Spectroscopy*, Wiley, 2004.

[12] M. Koch, R. Letrun and E. Vauthey, *Journal of the American Chemical Society*, 2014, **136**, 4066–4074.